SLAC – PUB – 3960
May 1986
(E/I)

A Magnetic Monopole Detector with Sensitivity to Extremely Small Magnetic Charge*

D. FRYBERGER, S. ST. LORANT, E. TILLMANN AND A. WOLFF

Stanford Linear Accelerator Center
Stanford University, Stanford, California, 94305

ABSTRACT

A magnetic monopole detector with a sensitivity range down to extremely small magnetic charge is described. Backgrounds in the detector are discussed and representative background distributions are given. Appropriate steps to minimize these backgrounds are detailed. The region of sensitivity of the detector to magnetic monopoles in terms of monopole charge and monopole mass is given.

Submitted to *Review of Scientific Instruments*

* Work supported by the Department of Energy, contract DE – AC03 – 76SF00515.

I. INTRODUCTION

In 1931 P.A.M. Dirac suggested[1] the possibility that a particle might exist which carries magnetic charge, giving theoretical impetus to an ongoing experimental effort to find magnetic monopoles. In that same paper Dirac also derived a relationship between electric and magnetic charges:

$$\frac{eg}{\hbar c} = \frac{n}{2} \quad , \tag{1}$$

where n is an integer; $\hbar$ and c have their usual significance. Using the value of the electron charge (which satisfies $\frac{e^2}{\hbar c} \cong \frac{1}{137}$) in Eq. (1) yields the Dirac unit of magnetic charge,

$$g_D \cong 68.5e \quad , \tag{2}$$

the smallest nonzero value of magnetic charge which satisfies Eq. (1). As a result of Eqs. (1) and (2), the notion that magnetic monopoles would carry a large charge, one or more Dirac units, has dominated almost all experimental searches. To date, no confirmed evidence for such a particle ever been presented, and the limits on its possible occurrence continue to decrease.[2]

The purpose of this paper is to describe the apparatus of an experiment which adds diversity to the on-going searches for particles carrying ng_D. Specifically, the sensitivity of this experiment ranges from well above the usual Dirac charge down to extremely small magnetic charges, *i.e.* down to $\sim 10^{-8} g_D$. Below $\sim 10^{-2} g_D$ is virgin territory and as such is the experimental motivation for this effort.[3]

II. EXPERIMENTAL APPARATUS

Briefly the approach of this experiment is to extract monopoles from a source and magnetically accelerate them into a detector.[5] While the experimental set-up can be configured in various ways, we describe here only the most recent configuration, which consists of four basic components: source, accelerator, sweeping magnet, and detector; the arrangement of these components is depicted in Fig. 1.

The source is a (commercially available) tungsten filament onto which monopoles or samples thought to contain monopoles may be placed. One technique for doing this is the use of a vacuum furnace, depicted in Fig. 2.

The sample to be investigated for monopole content is placed in the furnace crucible, which is heated by passing a dc current through a (commercially available) tungsten basket heating coil. The heat evaporates monopoles from the sample, and the magnetic field from the coil then propels them upwards through a deceleration coil (which reduces the monopole velocity) toward the mirror coil, set at $\sim 45°$. The mirror coil "reflects" the monopoles out of the upward moving stream and directs them horizontally into a recessed chamber housing the (source) filament. It is assumed that monopoles that hit the filament will remain deposited on its surface. The appropriate pole of a small permanent magnet is placed inside the filament to the enhance collection efficiency. Furnace trajectory calculations indicate that this increases the furnace efficiency by a factor ~ 7. Placing the filament in a recess protects it from contamination by the general evaporation products from the sample.

Assuming that the crucible is hot enough to evaporate monopoles from the sample,[7] the efficiency of the monopole transport and deposition is estimated to be about 1%, which includes the enhancement of the collection dipole. While this may seem low, one should note that the solid angle subtended by a filament at a distance of the trajectory path length in the furnace, ~ 30 cm, is $\sim 10^{-4}$ of 4π steradians. By connecting the external furnace coils, *i.e.* the deceleration and mirror coils, in series with the heating coil, this efficiency is insensitive to the heating current, the magnitude of the monopole charge, or its mass. The sign of the monopole charge to be collected is chosen by selecting the direction of the current through the three furnace coils and also the orientation of the collection dipole at the filament.

For a data run, the filament is first exposed in the furnace and then transferred to the main apparatus where it is used as the source as shown in Fig. 1.

Electrically heating this filament with a dc current, then drives the monopoles off of the filament, making them available for acceleration. When the current in the superconducting solenoidal accelerator magnet $I_{sc} = 400$ A, the magnetic field at the location of the source filament is ~ 300 G. This field is several times greater than the largest field associated with the filament heating current and the capture of evaporated monopoles into the acceleration field is assured. Trajectory calculations indicate that monopoles thus captured will enter the electron multiplier tube (EMT) aperture, approximately 1.2×1.0 cm^2 in area.

The accelerator consists of a superconducting solenoidal magnet with a 7 cm warm bore.[8] The external physical length of the dewar is 2.22 m. The current in the solenoid produces a central field B_0 in the ratio 113 G/A; the effective magnetic length ℓ is 176 cm. At a current of $I_{sc} = 400$ A, for example, $B_0 = 45.2$ kG and $\int B d\ell = 8 \times 10^6$ G-cm.

The solenoidal magnetic field will accelerate magnetic monopoles along the magnetic axis, imparting to them a kinetic energy (in electron volts)

$$KE = 300 B_0 \ell g/e \quad , \tag{3}$$

where the factor 300 converts statvolts to volts and g/e is the monopole's magnetic charge normalized to the electron charge. It is interesting to note that Eq. (3) indicates that for Dirac monopoles and a current of 400 A we have a 164 GeV accelerator.

The monopole "beam" then passes between the poles of a small magnet which is used to sweep out any ions or electrons which may also be travelling down the solenoid. At its maximum current of 10 A this sweeping magnet has a central field of 586 G and an $\int B d\ell$ of 1.44×10^4 G-cm. The monopoles which have been accelerated by the main solenoidal field will continue through the sweeping magnet toward the detector, being deflected on the order of a milliradian. The associated transverse displacement of the monopole track at the EMT is $\lesssim \frac{1}{2}$ mm and may be ignored.

The beam then enters a 16 stage Hamamatsu R-596 EMT where it is detected. The EMT assembly, which includes two cylinders of magnetic shielding, is located inside a coil that bucks out the fringe field from the accelerator magnet. The sum of the bucking and fringe fields is monitored outside the vacuum pipe at the EMT location as indicated in Fig. 1. Knowledge of the field at this location is important because the gain of the EMT is affected by magnetic field leaking through the magnetic shielding. In an effort to eliminate gain variation of the EMT due to leakage flux variations, the main solenoid and the bucking coil are both computer controlled and are ramped together at a constant current ratio to the chosen operating point.

The EMT anode signal is fed through a low noise blocking capacitor. This feature enables one to set independently the voltage on the first dynode and total voltage across the dynode chain V_{EMT}: as will be seen below, the former has a significant effect on background counts while the latter controls the tube gain. V_{EMT} has been arbitrarily standardized at 3000 volts.

The source and the EMT are in a common vacuum system to eliminate the possibility that monopoles of small charge might not have very much penetrating power. This design feature, however, entails the disadvantage that outgassing from the filament or from any sample heated by the filament will raise the pressure in the EMT. The use of the vacuum furnace to evaporate monopoles out of samples and onto the filament prior to its installation into the detector apparatus essentially eliminates this outgassing problem. Consequently, while the use of a furnace entails an additional step in the experimental procedure with its attendant uncertainties, it enables the processing of greater quantities and varieties of samples.

During the data and background runs the vacuum in the system can be easily maintained at $\leq 10^{-5}$ torr, which implies a mean free path of ≥ 5 m, comfortably in excess of the ~ 3 m path from source to EMT. Such a vacuum is more than adequate to satisfy the EMT operational requirement of 10^{-4} torr.

The signals from the EMT are amplified and fed into the q input[10] of a LeCroy Model 3001 qVt multichannel analyzer, which in turn feeds its data to a PDP-11. Some on-line analysis is performed in the PDP-11, and the data are then transmitted to the SLAC IBM 3081 computer system for off-line analysis.

The gain of the electronics is measured by observing the qVt distribution resulting from 20 ns FWHM test pulses fed into the amplifier. The gain and stability of the data collection system as a whole is monitored by the observation of the qVt spectra associated with photon beams and/or ion beams. For this purpose, the first and second moments of the qVt distributions are routinely calculated on-line after each data and background run.

The first moment is defined by

$$m_1 = \frac{\sum_i i\, n_i}{\sum_i n_i} \tag{4}$$

and the second moment by

$$m_2 = \frac{\sum_i i^2\, n_i}{\sum_i n_i} \quad , \tag{5}$$

where i is the channel number ($0 \leq i \leq 1023$), and n_i is number of counts in the i^{th} channel.

III. BACKGROUND

There are several sources of background that can cause signals from the EMT. These signals will give counts in the qVt, the distribution of which depends upon the source of the background and the settings of various parameters of the experimental apparatus. These sources include the following:

1. general background
2. electrons
3. ions
4. photons

These backgrounds have been studied throughout the parameter space of the experimental apparatus, and the results of these studies are described below.

General Backgrounds

With appropriate settings the general background rate, due to cosmic rays, tube noise, local radioactivity, *etc.*, can be reduced to less than one count/minute (summed over all channels). The most important parameter here is the voltage V_1 on the first dynode and entrance grid (electrically joined in the R-596) of the EMT; if V_1 is kept negative, it will repel free electrons (and negative ions) in the vacuum system, and if it is kept small ($|V_1| < 100$ V) the efficiency for positive ions to generate a secondary electron is very small. A typical general background distribution, labeled "Cosmic Rays," is plotted in Fig. 3. Although this background is not serious for short data runs, it does set a lower limit of sensitivity for monopole counts in the qVt spectrum.

Electrons

Although a hot filament is well known to be a copious source of electrons, this possible source of background can be eliminated by making V_1 negative, precluding (low energy) electrons from entering the dynode chain. This negative potential also eliminates negative ions as a source of background. The setting $V_1 = -50$ volts was selected for data runs. On the other hand, a negative potential will attract positive ions and some care must be devoted to the control of the positive ion background.

Positive Ions

It is well known that positive ions are emitted from a heated filament.[11] These consist of ionized atoms of the source material as well as those of various impurities it may contain. At relatively low temperatures, the emission rates and the proportions of the different ion species can vary greatly. One can enhance the positive ion counting rate by setting the filament to a positive voltage to give the positive ions an initial kinetic energy and by setting V_1 to ≤ -1000 V to enhance secondary electron emission at the first dynode. A typical "enhanced" ion count rate curve versus filament current I_F (and an estimated filament temperature) is given in Fig. 4. We note that the currents in this plot are below that at which there are enough ultraviolet photons to give any qVt counts (see Fig. 10).

One means of controlling the ion count rate is by varying the filament to ground potential. A typical ion count rate curve versus the voltage on the (positive terminal of the) filament with respect to ground is given in Fig. 5. The abrupt rise in rate in the range $4 < V_0 < 7$ volts is associated with the ionization work function of the major ion in the beam.[12] The width of this step is presumed to be due mostly to the 0.8 volt drop across the filament at 18 A. It is important to note that when V_0 is less than the ionization work function, that emission of ions from the filament is highly suppressed and, in fact, for $V_0 \sim 0$, the positive ion count rate is very close to the general background rate of ~ 1 count/min.

The ion count rate versus (minus) the first dynode voltage V_1 (keeping total EMT voltage constant) is plotted in Fig. 6. This curve indicates that the sensitivity of the EMT to positive ion counts is essentially eliminated by operating the first dynode at -50 V. As can be seen from Fig. 6, this step reduces the ion count rate to essentially that of the general background. That the first dynode voltage should effect the ion count rate so dramatically is quite understandable, since in this experimental apparatus this voltage or potential is the major source of the kinetic energy with which the ion strikes the first dynode; the only other source is the filament offset voltage (less the ionization work function), which for

the curve in Fig. 6 contributes ~ 4 volts.

For selected values of V_1, the spectral distributions of the ion counts are given in Fig. 7. The increase in pulse height with an increase in $|V_1|$ is clearly manifest. A plot of the first moments of some ion distributions versus V_1 is given in Fig. 8. From Fig. 6 we see that the probability that an ion will generate secondary electrons drops precipitously for $V_1 \lesssim -400$ volts. From the location of the "Photon Calibration Point" connected by the dashed extension to the values of the first moments in Fig. 8, we conclude that the probability of the emission of more than one secondary election tends to vanish as the probability of detection drops. In fact, the data plotted in Fig. 8 indicates that for $|V_i| \leq 200$ V pulses from the later dynode stages, rather than the first stage, are the major source of the qVt distributions; the first moment of these distributions becomes significantly smaller than that associated with a single photo electron.

It is clear from the above discussion that even at low temperature, a filament can be a copious source of ion counts in the EMT and effective steps must be taken to control this background. The first step is to set V_0 less than the ionization work function, which suppresses the emission process. Figure 5 indicates that this step, grounding the positive terminal of the filament, affords a suppression factor of $\geq 10^5$. The second step is to suppress the detection process. From Fig. 6, we see that setting $V_1 = -50$ volts affords another suppression factor of $\geq 10^5$.

The sweeping magnet is one more tool for the understanding and control of the positive ion background. In order to understand the effectiveness of the sweeping magnet, the qVt counts due to ions were studied as a function of sweeping magnet current I_S. In Fig. 9 this rate is plotted for $0 \leq I_S \leq 5$ A. The narrow peak at 0 A is due to the beam moving directly from the source filament to the first dynode of the EMT. Once the sweeping magnet current is high enough to prevent the direct beam from entering the EMT, (~ 0.5 A) one sees a broad shoulder with a rate of $\sim 2\%$ of the direct beam. This shoulder, attributed to

ions scattering off the vacuum pipe walls, is reduced to the general background level by $I_S \sim 5$ A, one half of the maximum allowable current in the sweeping magnet. Comparison of this background level to the direct beam rate shows that the sweeping magnet affords an attenuation factor $\geq 10^4$. The fact that the sweeping magnet is not essential to eliminate positive ion counts (As described above, the proper setting of V_0 and V_1 affords an attenuation factor of $> 10^5 \times 10^5 = 10^{10}$.) enables one to use I_S to investigate the amount of ion content in qVt data or background distributions.

It is important to note here that when the monopole accelerator magnet is on, the axial field channels ions from the filament to the EMT with an enhanced efficiency, thereby increasing system vulnerability to this source of background. This effect is especially pernicious since it tends to result in counts which correlate with the presence of the acceleration field, just as one supposes valid monopole counts would do. This ion beam enhancement factor has been measured. It rises quickly, even at small I_{sc}; at $I_{sc} = 1.2$ A, there is already an enhancement by a factor 10. The effect saturates by $I_{sc} = 100$ A and remains flat out to $I_{sc} = 400$ A at a factor of ~ 100. With the two suppression factors of 10^5 discussed above, and the ability to use the sweeping magnet to check residual ion contamination, this ion collection enhancement is not a serious problem.

Photons

The photon induced background rate in the EMT does not become significant until $I_F \sim 50$ A. Figure 10 gives a rate curve of the total photon count rate in the qVt vs. I_F. As one would expect, these rates were found to be independent of I_{sc}. In Fig. 11 are given m_1 and $\sqrt{m_2}$ for some qVt spectra of photon induced background as a function of I_F. The ion background in these spectra was eliminated, as discussed above, by setting $V_0 = 0$, $V_1 = -50$ V, and $I_S = 5$ A. The fact that m_1 and $\sqrt{m_2}$ are not functions of I_F indicates the spectral shapes are independent of I_F, even though the rate varies by more than two orders of

magnitude (in the region, $I_F > 60$ A). In a similar way we also established that the spectral shape of the photon qVt distribution is also independent of I_{sc}.

In Fig. 3 a typical photon qVt distribution is given. Note that while the high number of counts in the lower channels tends to obscure attendant monopole counts in that region, the spectrum is void above channel 510, and even a few monopole counts in this latter region would be noticed. If one assumes that the monopole qVt distribution would resemble that of a 2 kV ion beam, say, then ~5% of the monopole distribution would appear above channel 510. Consequently, such a monopole distribution containing 100 counts would permit the unambiguous detection of monopoles by inspection. Such a monopole distribution containing fewer counts could be identified by fitting the data spectrum (photons plus monopoles) to the known shapes of the (photon) background spectra. The efficacy of such a procedure would, of course, depend upon the number of counts in the data spectrum and to what extent the monopole spectrum differed from the background spectrum, which in the case of photons is characterized by single photoelectron emission from the first dynode.

IV. CONCLUSION

The above sections have described a device capable of detecting magnetic monopoles of very small charge. The operation is straightforward; the monopoles are evaporated from a filament and then accelerated in a vacuum by a large solenoidal magnetic field into an EMT, where they are detected. It is the large amount of energy which the solenoidal magnetic field can transfer to a magnetic charge that enables this apparatus to be sensitive to such small magnetic charges.

By the study of ions emitted from the source filament, it was shown that the ion detection probability becomes significant when the ion has ~ 400 keV of kinetic energy. In order to estimate the minimum charge of a monopole which this apparatus could detect, we arbitrarily multiply this number by a factor ten, specifying 4 keV of kinetic energy as necessary for monopole detection. Using

this value (and $I_{sc} = 400$ A) in Eq. (3) yields a minimum detectable magnetic charge of $2.5 \times 10^{-8} g_D$. This limit is indicated in Fig. 12.

In order to be detectable, we also assume that the monopole velocity at the EMT must be equal to or greater than that of a 4 keV tungsten ion ($\beta \cong 2 \times 10^{-4}$). This latter assumption specifies the maximum mass of a detectable monopole as a function of monopole charge. This velocity limit is also indicated in Fig. 12.

One can see that while this apparatus cannot accelerate a massive Grand Unified Monopole (GUM) to a detectable velocity, there are other possibilities which do fall within the range of sensitivity of this apparatus, *e.g.* a vorton atom,[13] or an electroweak monopole.[14] Finally, of course, one must add that as with all such experimental searches the putative monopole must satisfy a variety of assumptions to be detected. If monopoles are detected, these assumptions are not a problem; the fact of detection verifies them. However, if monopoles are not detected, one is never sure whether the reason is that monopoles are not present in the samples in the requisite numbers, or that they are there but do not satisfy some assumption which is necessary for the experimental process to lead to detection. Thus, negative results are not fully conclusive but rather they furnish motivation to improve or vary the detection method.

ACKNOWLEDGEMENTS

We are indebted to numerous people for the loan of various pieces of apparatus used in the detector assembly. We in particular wish to thank E. Gruenfeld and W. Kapica for their skills in the construction and assistance in the operation of the detector and D. Alzofon for his contribution to earlier phases of this effort.

REFERENCES and FOOTNOTES

1. P.A.M. Dirac, *Proc. Roy. Soc.*, A133, 60 (1931).

2. See, *e.g.,* the recent review by D.E. Groom, "In Search of the Supermassive Magnetic Monopole," *UUHEP 85/8*, October 15, 1985, Submitted to *Physics Reports*; Some earlier review papers are: G. Giacomelli, "Magnetic Monopoles," CERN-EP/84-17, February 17, 1984, contribution to the First ESO-CERN Symposium, Geneva, 21-25 November 1983; R.A. Carrigan, Jr., and W.P. Trower, *Nature*, 305, 673 (1983); B. Cabrera, and W.P. Trower, *Found. of Phys.*, 13, 195 (1983).

3. Searches in the region of small magnetic charge were suggested some years ago by Usachev,[4] who at the same time pointed out that all of the derivations of Eq. (1) had flaws and should not be fully trusted.

4. Yu. D. Usachev, *Fiz. Elem. Chast. At. Yad.*, 4, 225 (1973) [*Sov. J. Part. and Nucl.*, 4, 94 (1973)].

5. The basic idea of this detector is the similar to that used in some previous quark searches;[6] the principal difference is that magnetic (rather than electric) acceleration is employed.

6. W.A. Chupka, J.P. Shiffer, and C.M. Stevens, *Phys. Rev. Lett.*, 17, 60 (1966); C.M. Stevens, J.P. Shiffer, and W. Chupka, *Phys. Rev.*, D14, 716 (1976).

7. With a B11-3×.040W basket heater and a C6 crucible (R.D. Mathis Company) the furnace can heat a sample to $\sim$ 1100°C.

8. This magnet was (one of four) originally designed and built at Argonne National Laboratory as a proton spin tipping magnet.[9] When the ANL program was shut down, the magnet became surplus. It was then shipped to SLAC for the purpose of this monopole search program.

9. S-T. Wang, K. Mataya, A. Paugys, and C.J. Chen, *IEEE Trans. Magn.*, MAG-15, 107 (1979).

10. The q input distributions of the qVt are analyzed by pulse charge (*i.e.* area) while the V input distributions are by height. This distinction is academic, however, since the pulse width of an EMT pulse is not a function of the magnitude of the pulse, but rather of the time constants of the circuitry.

11. L.P. Smith, *Phys. Rev.*, 35, 381 (1930); P.B. Moon, *Proc. Camb. Phil. Soc.*, 28, 490 (1932). The fact that the curve in Fig. 4 is not "smooth," results from slight variations in the time allowed for "settling" after a change in I_F. A smoother curve would be obtained by allowing generous settling times (*i.e.* one or more hours) between points.

12. We note that Smith (Ref. 11) finds for tungsten an ionization work functions of 6.55 V, while Moon (Ref. 11) estimates it to be about 7.1 volts.

13. D. Fryberger, *IEEE Trans. Magn.*, MAG-21, 84 (1985).

14. Such a particle might be expected, for example, in the S0(3) theory explored by G. 't Hooft, *Nucl. Phys.*, B79, 276 (1974).

FIGURE CAPTIONS

1. Experimental Apparatus.

2. Depiction of vacuum furnace for evaporating monopoles from a sample and depositing them on a source filament. The coils are shown as connected for north monopole extraction. A typical monopole trajectory is shown. The dipole used to enhance monopole collection is not shown.

3. Pulse height distributions of various backgrounds. The points labelled "Cosmic Rays" total 435 counts and are the sum of 10 runs which total 700 min. The ten counts in the last bin are due to the inclusion of channel 1023 (the final channel) which has no upper limit on pulse height. The points labelled "Photon Beam" total 140 thousand counts and are from a four minute run with $I_F = 70$ A. As discussed in the text, the ion counts were suppressed for this photon beam spectrum by the following settings: $V_0 = 0$ V, $V_1 = -50$ V, and $I_S = 6$ A.

4. Plot of the qVt ion count rate versus filament current I_F. That the curve is not smooth in the vicinity of $I_F \sim 17$ A is indicative of the variability of ion emission even under nominally the same conditions.[11] Filament temperatures as estimated from the manufacturers nomograph are indicated. At a given current, the filament temperature, of course, is not uniform; the ends are cooled by thermal conduction to the lead supports, and the center tends to be heated by radiation and conduction from the adjacent turns.

5. Plot of qVt ion count rate versus filament offset voltage V_0. V_0 is the voltage of the positive filament terminal with respect to ground.

6. Plot of the qVt ion count rate versus the first dynode voltage V_1 of the EMT.

7. Plot of the qVt distributions for ion beams for selected values of the first dynode voltage V_1. These distributions were each accumulated in a one

minute run. For $V_1 \lesssim -2000$ volts, one can see an accumulation of counts in channel 1023.

8. Plot of the first moment m_1 of the qVt distributions of ion beams as a function of (minus) V_1. The "Photon Calibration Point" is the value of the first moment of a photon distribution (due to a single photoelectron) with $V_{\rm EMT} = 3000$ volts. The dashed line is extended through the first moments of the ion distributions to the photon calibration point to indicate the location of the moment associated with a distribution generated by a single secondary electron. Evidently the distributions associated with $V_i \leq -200$ V are mainly due to background pulses generated in later dynodes of the EMT, which pulses do not benefit from all 16 stages of multiplication.

9. Plot of the qVt ion count rate versus the sweeping magnet current I_S.

10. Plot of qVt photon count rate versus filament current I_F. As in Fig. 4, the filament temperature as a function of I_F is estimated and is indicated at the top of the figure. The ion background counts were suppressed as in the photon distribution shown in Fig. 3.

11. Plot of the spectral moments m_1 and $\sqrt{m_2}$ of photon qVt distribution as a function of I_F. Instead of m_2, it is more informative to compare $\sqrt{m_2}$, the rms of the distribution, to m_1; from the defining equations, Eqs. (4) and (5), one sees that m_1 and $\sqrt{m_2}$ can both be thought of as channel numbers. (m_2 is like the square of a channel number.) The ion background counts were suppressed as in the photon distribution shown in Fig. 3.

12. Plot showing the region of sensitivity of this monopole detector, with monopole charge and monopole mass as coordinates. The tungsten ion calibration point, which is used as a reference to define the limits of the region of monopole detectability, is also indicated.

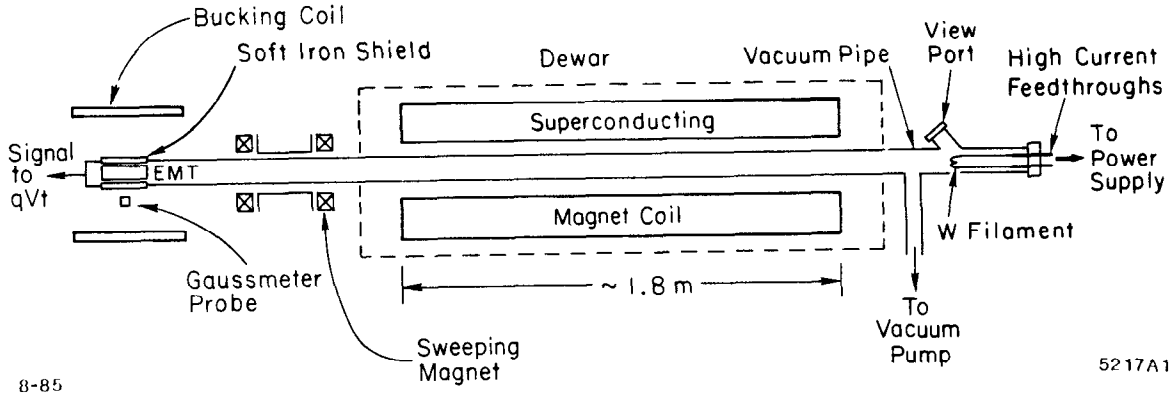
Bucking Coil
Soft Iron Shield
Dewar
Vacuum Pipe
View Port
High Current Feedthroughs
Superconducting
Signal to qVt
EMT
To Power Supply
Magnet Coil
W Filament
Gaussmeter Probe
~ 1.8 m
To Vacuum Pump
Sweeping Magnet
8-85
5217A1

Fig. 1

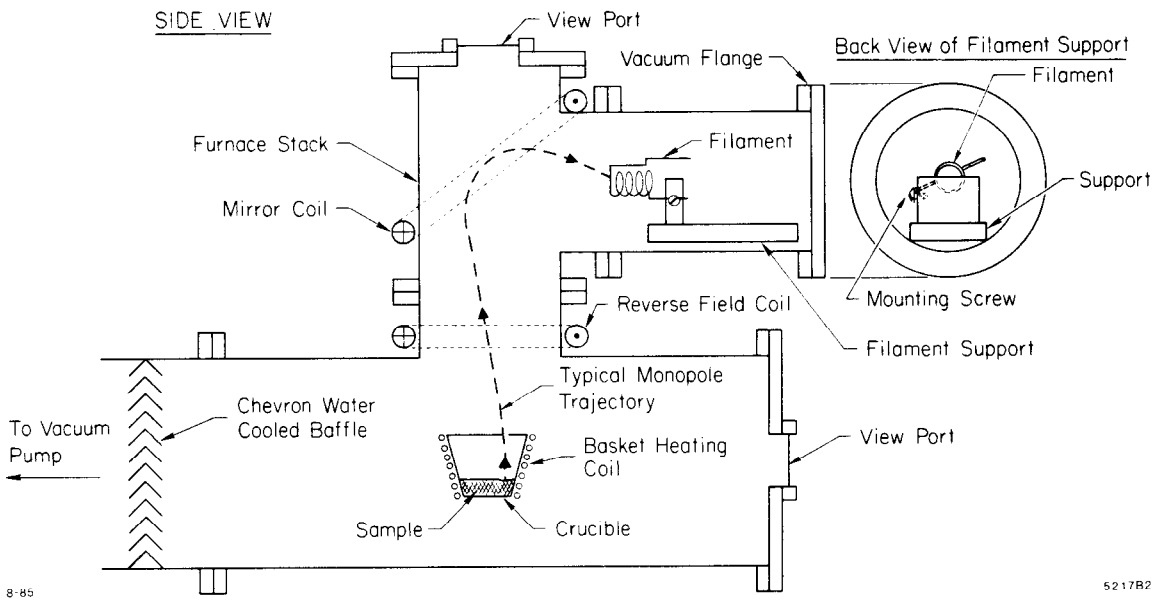
SIDE VIEW
View Port
Vacuum Flange
Back View of Filament Support
Filament
Furnace Stack
Filament
Support
Mirror Coil
Mounting Screw
Reverse Field Coil
Filament Support
Typical Monopole
Trajectory
To Vacuum
Pump
Chevron Water
Cooled Baffle
Basket Heating
Coil
View Port
Sample
Crucible
8-85
5217B2

Fig. 2

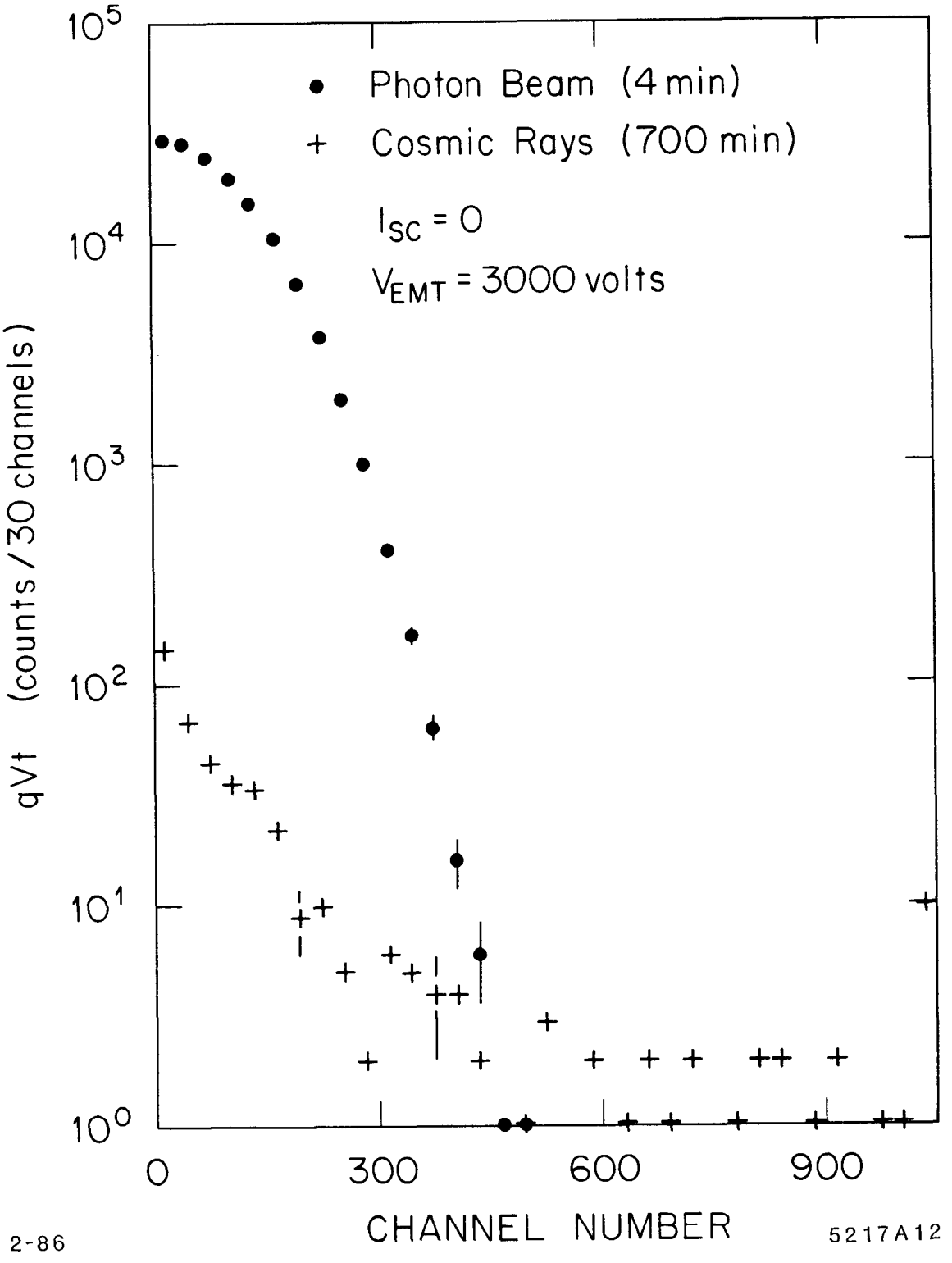
Photon Beam (4 min)
Cosmic Rays (700 min)
I_{SC} = 0
V_{EMT} = 3000 volts
qVt (counts / 30 channels)
10^5
10^4
10^3
10^2
10^1
10^0
0
300
600
900
CHANNEL NUMBER
2-86
5217A12

Fig. 3

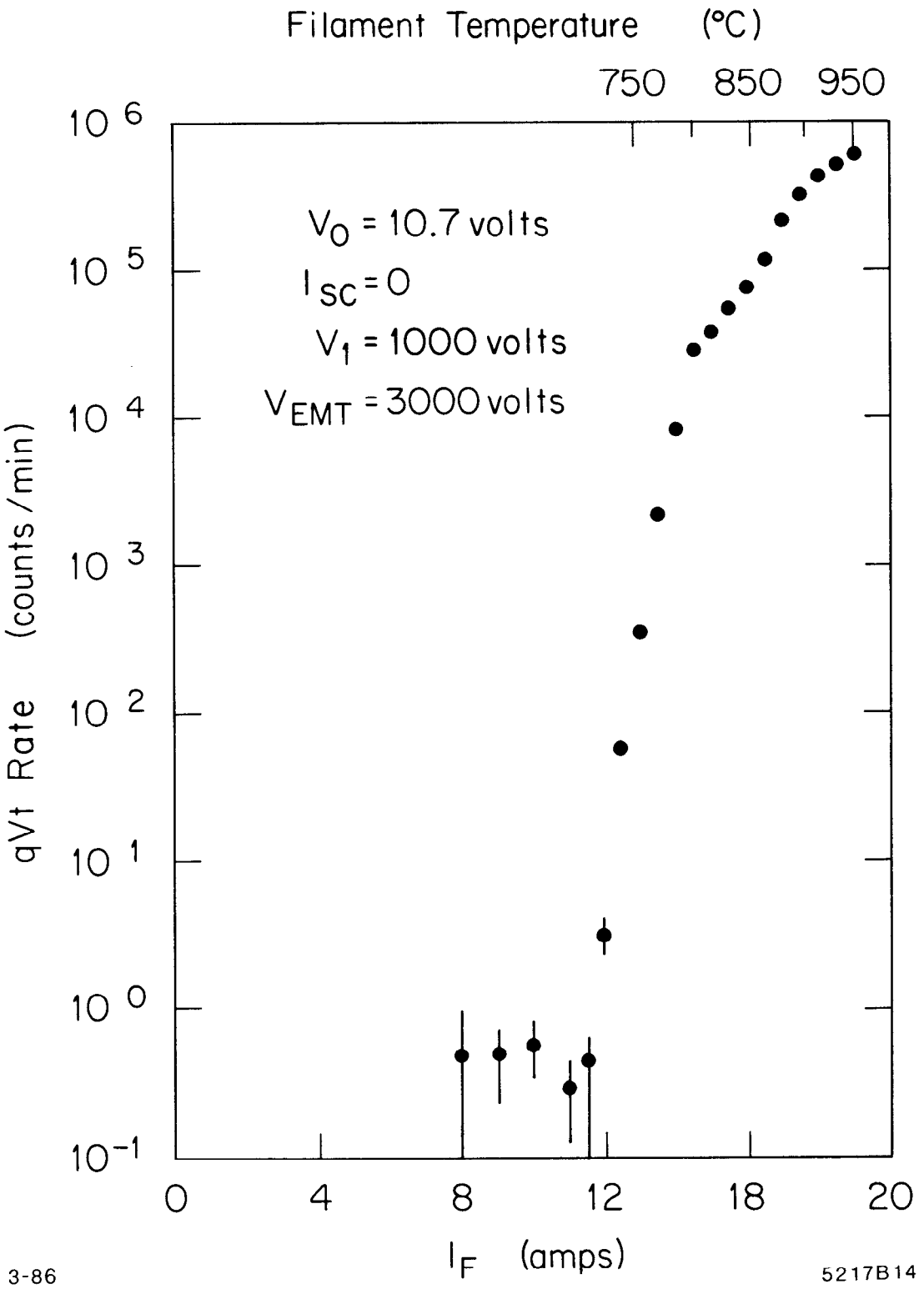
Filament Temperature (°C)
750
850
950
10^6
10^5
10^4
10^3
10^2
10^1
10^0
10^{-1}
V_0 = 10.7 volts
I_{SC} = 0
V_1 = 1000 volts
V_{EMT} = 3000 volts
qVt Rate (counts/min)
0
4
8
12
18
20
I_F (amps)
3-86
5217B14

Fig. 4

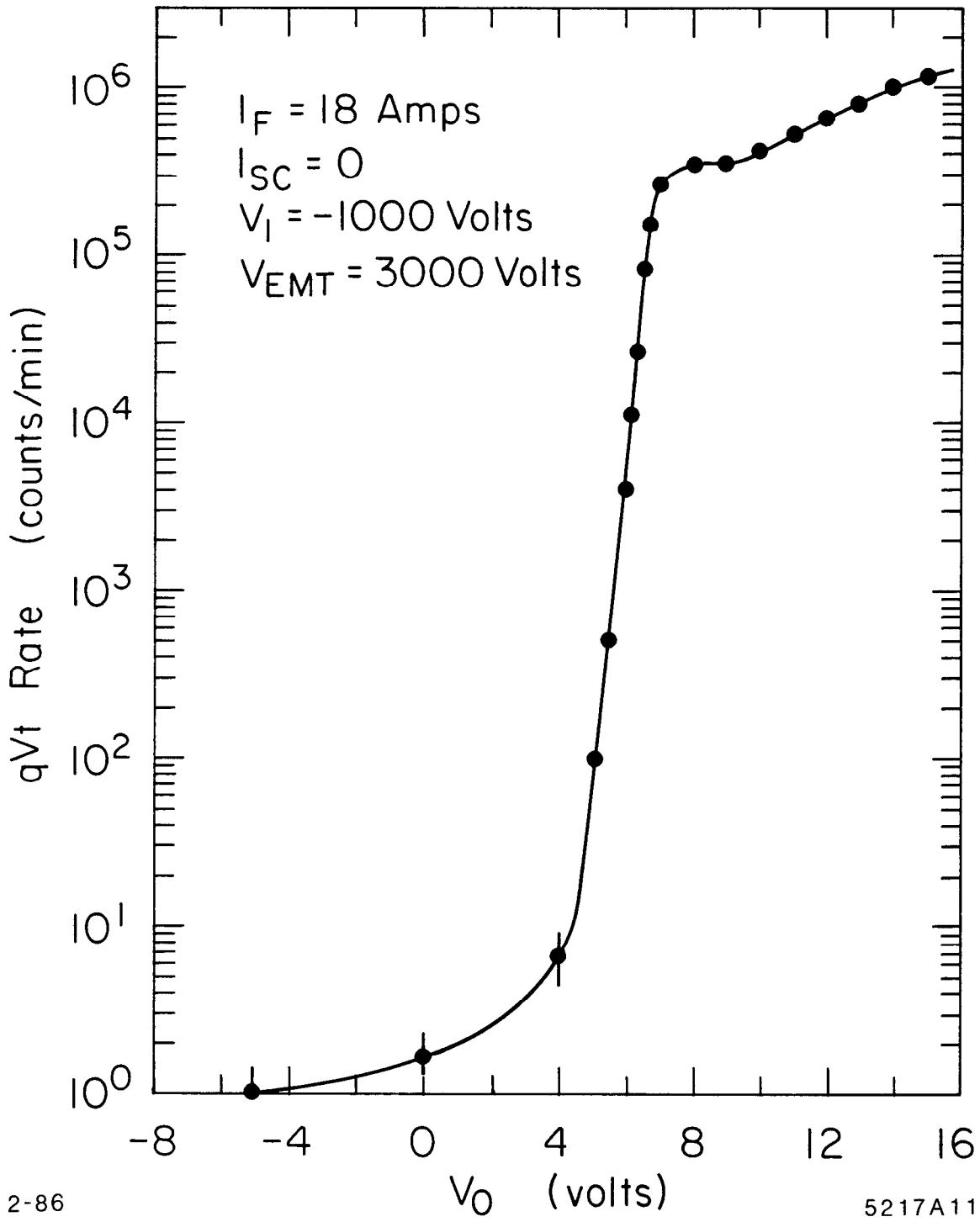
I_F = 18 Amps
I_{SC} = 0
V_I = −1000 Volts
V_{EMT} = 3000 Volts
qVt Rate (counts/min)
10^6
10^5
10^4
10^3
10^2
10^1
10^0
−8
−4
0
4
8
12
16
V_O (volts)
2-86
5217A11

Fig. 5

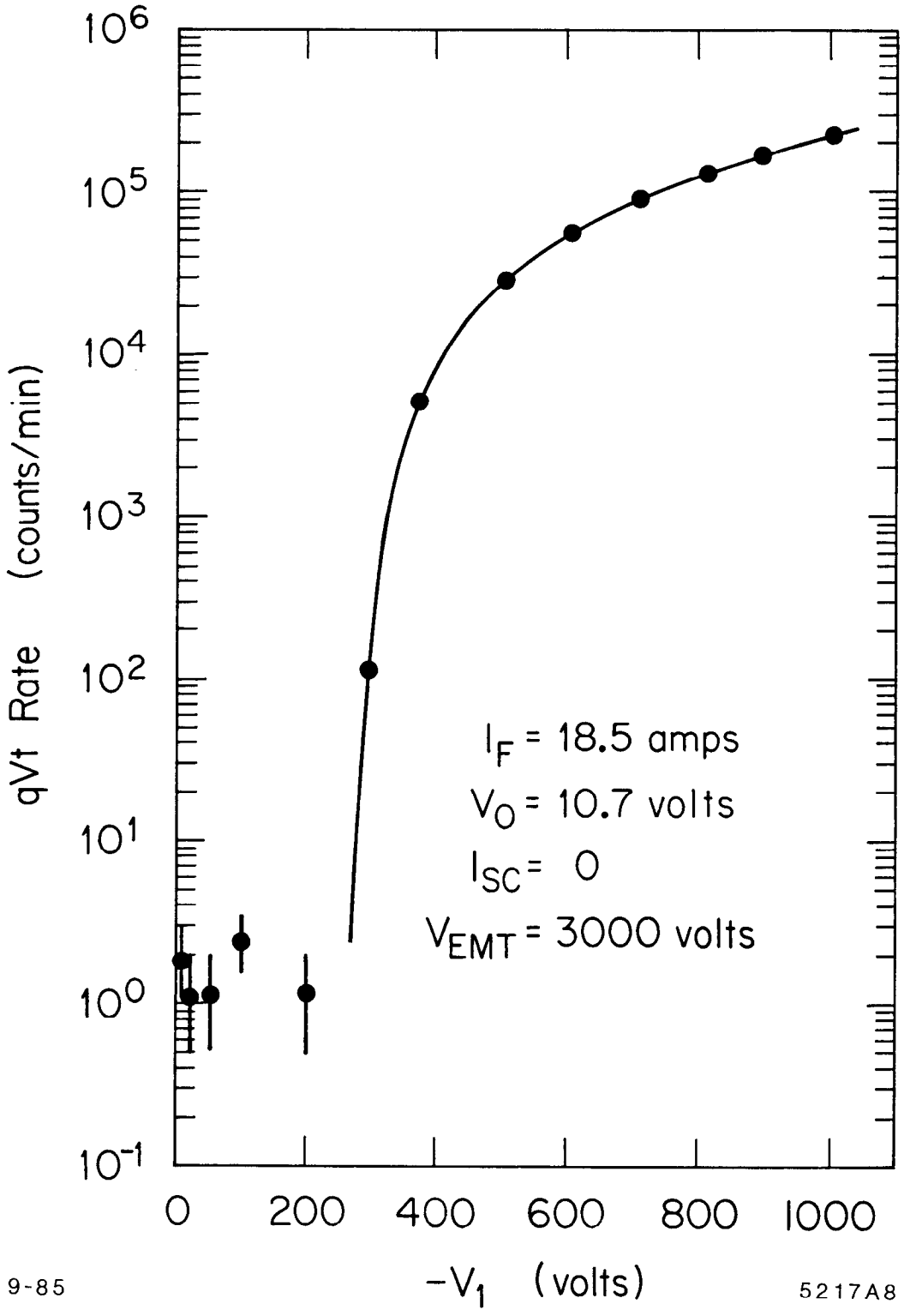
10^6
10^5
10^4
10^3
10^2
10^1
10^0
10^{-1}
qVt Rate (counts/min)
I_F = 18.5 amps
V_O = 10.7 volts
I_{SC} = 0
V_{EMT} = 3000 volts
0
200
400
600
800
1000
$-V_1$ (volts)
9-85
5217A8

Fig. 6

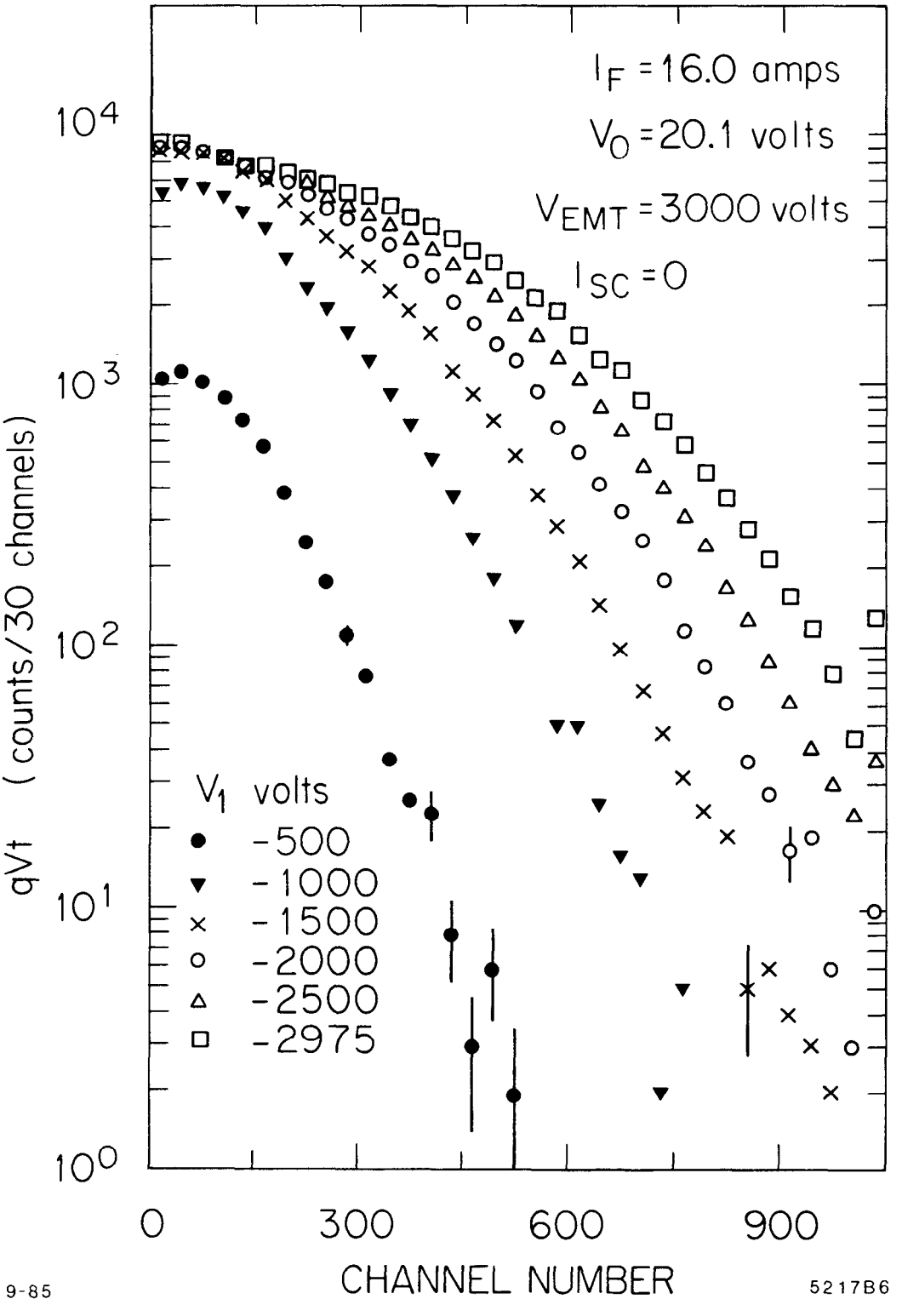
I_F = 16.0 amps
V_0 = 20.1 volts
V_{EMT} = 3000 volts
I_{SC} = 0
V_1 volts
-500
-1000
-1500
-2000
-2500
-2975
qVt (counts/30 channels)
10^4
10^3
10^2
10^1
10^0
0
300
600
900
CHANNEL NUMBER
9-85
5217B6

Fig. 7

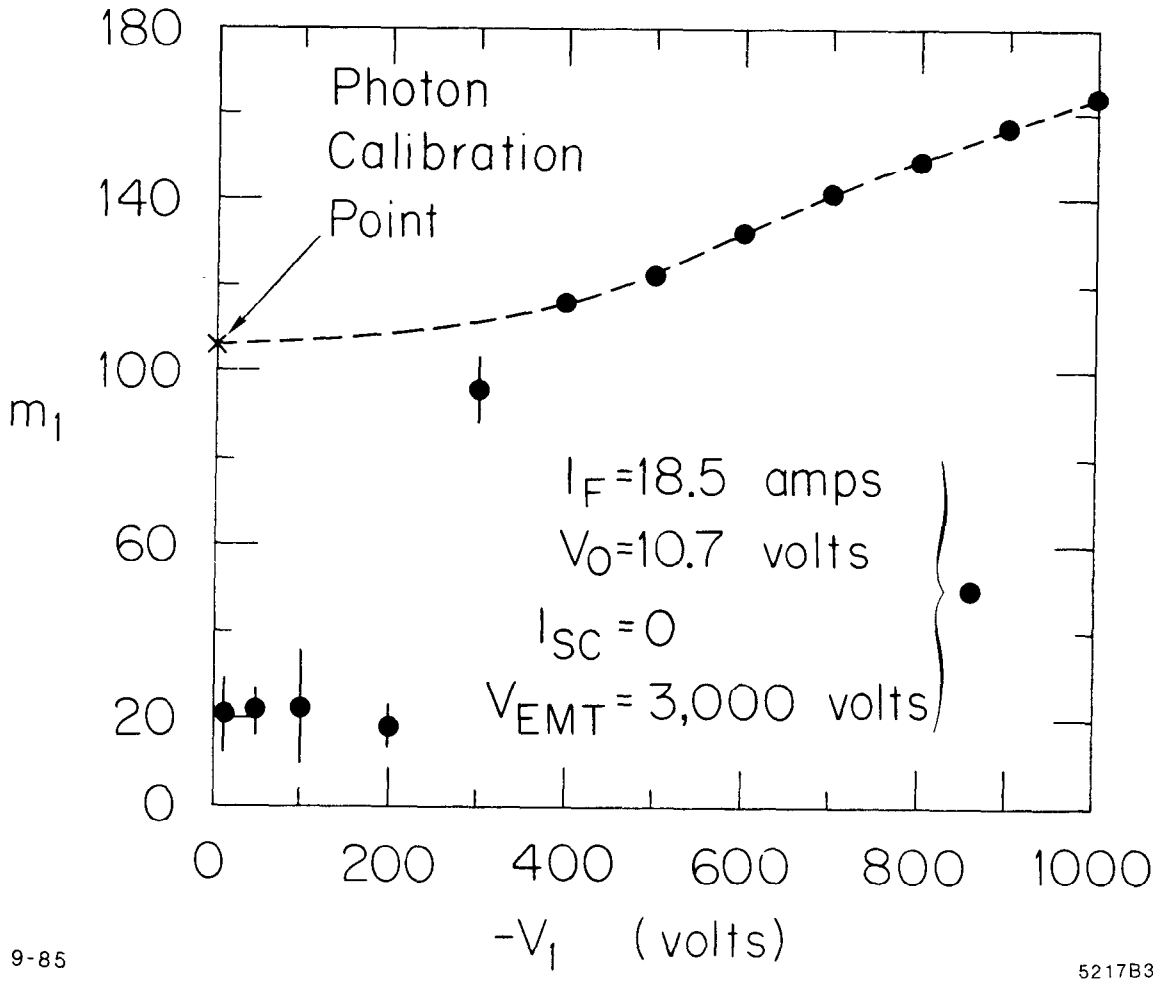
180
140
100
60
20
0
m_1
Photon
Calibration
Point
I_F=18.5 amps
V_O=10.7 volts
I_{SC} = 0
V_{EMT} = 3,000 volts
0
200
400
600
800
1000
$-V_1$ (volts)
9-85
5217B3

Fig. 8

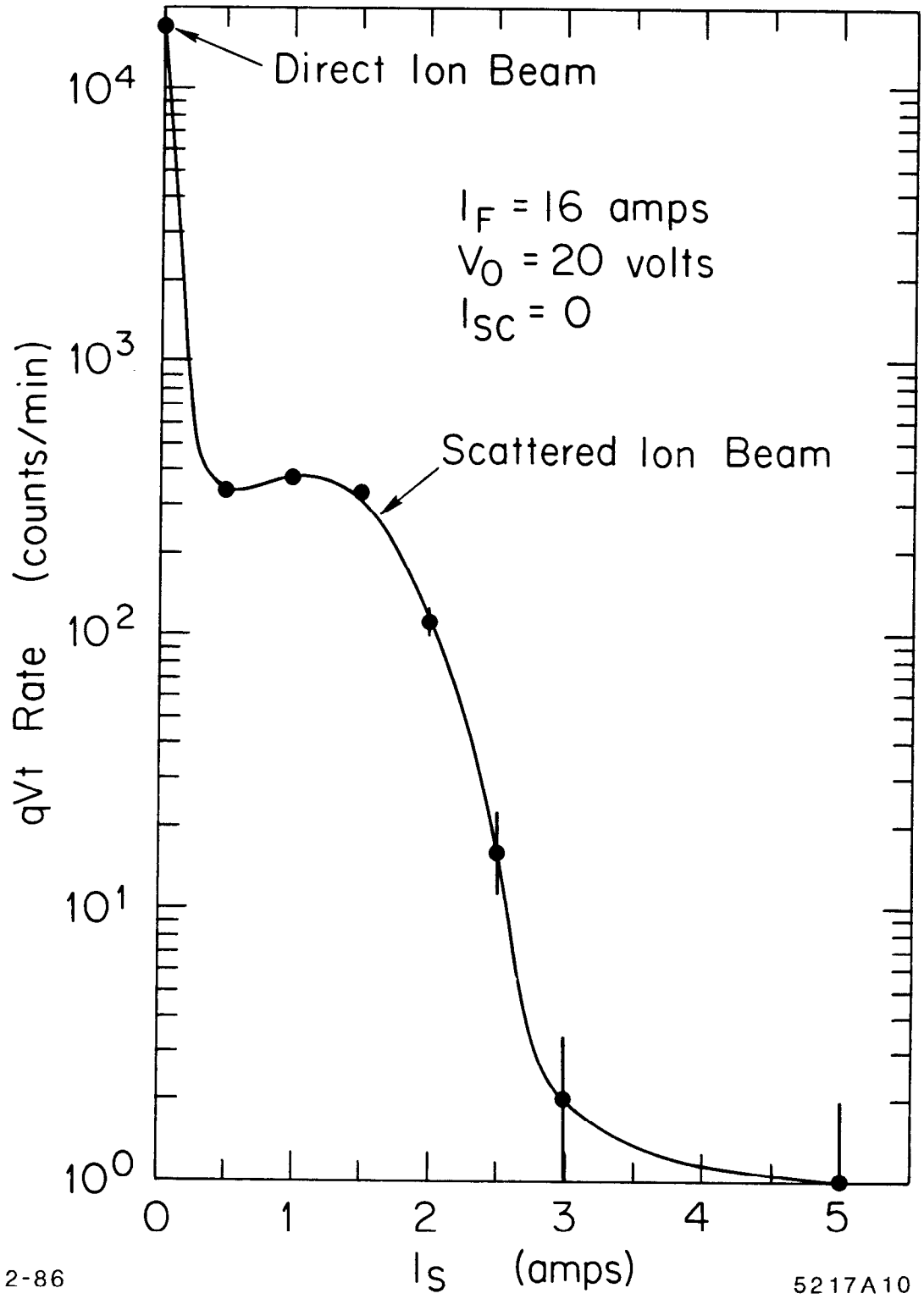
Direct Ion Beam
I_F = 16 amps
V_0 = 20 volts
I_{SC} = 0
Scattered Ion Beam
10^4
10^3
10^2
10^1
10^0
qVt Rate (counts/min)
0
1
2
3
4
5
I_S (amps)
2-86
5217A10

Fig. 9

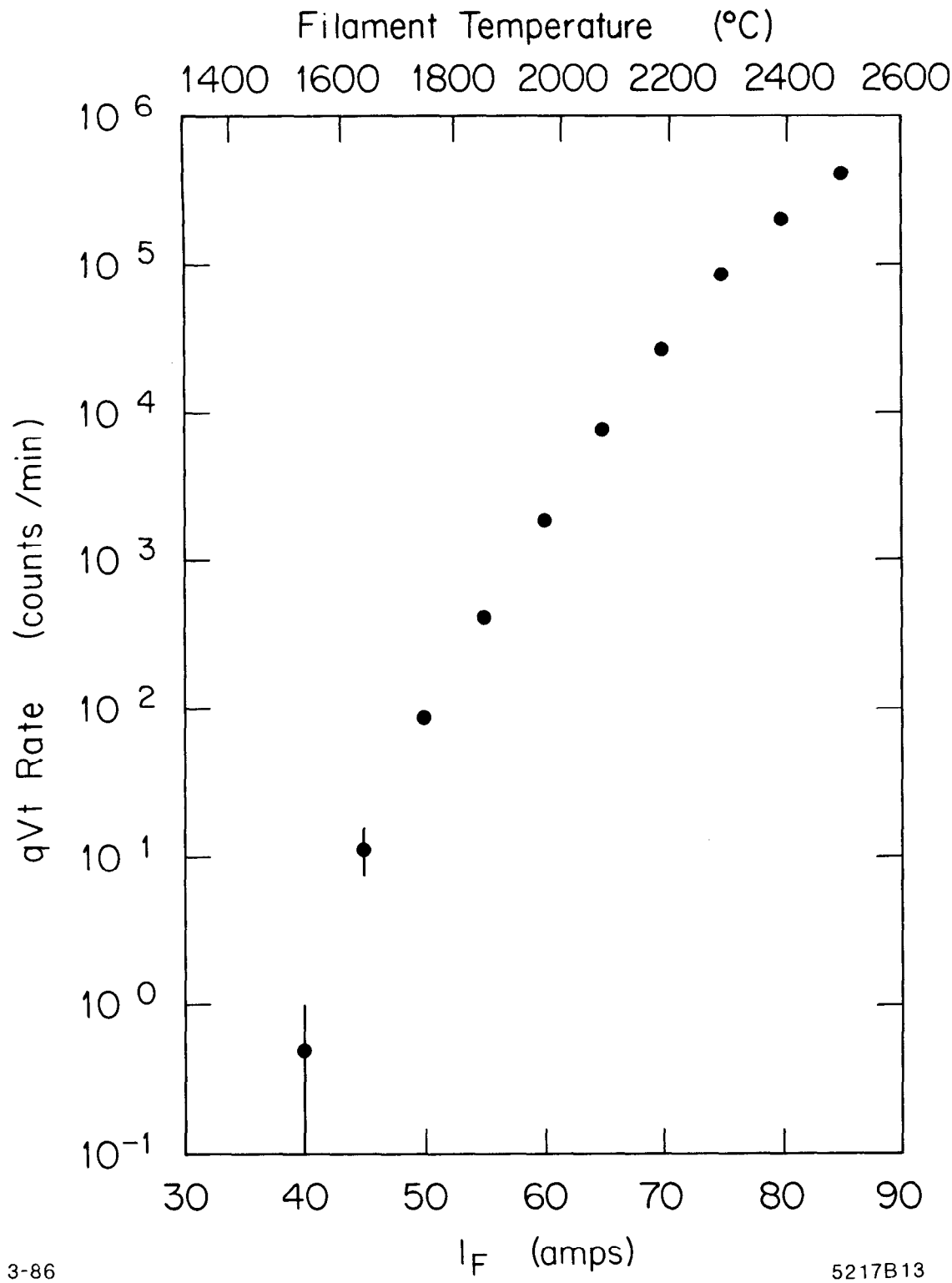
Filament Temperature (°C)
1400 1600 1800 2000 2200 2400 2600
10 6
10 5
10 4
10 3
10 2
10 1
10 0
10-1
qVt Rate (counts /min)
30 40 50 60 70 80 90
IF (amps)
3-86
5217B13

Fig. 10

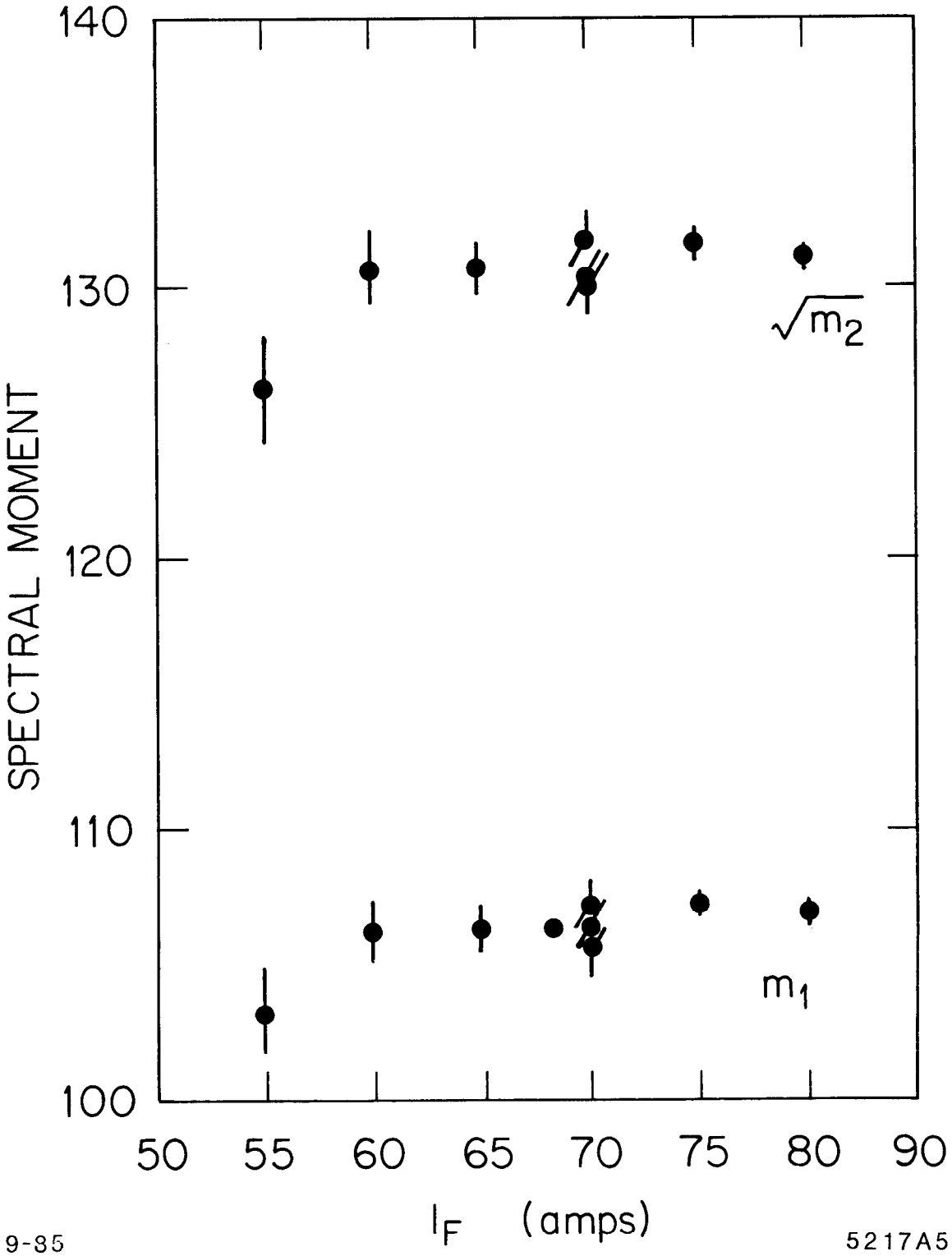
140
130
120
110
100
SPECTRAL MOMENT
$\sqrt{m_2}$
m_1
50
55
60
65
70
75
80
90
I_F (amps)
9-85
5217A5

Fig. 11

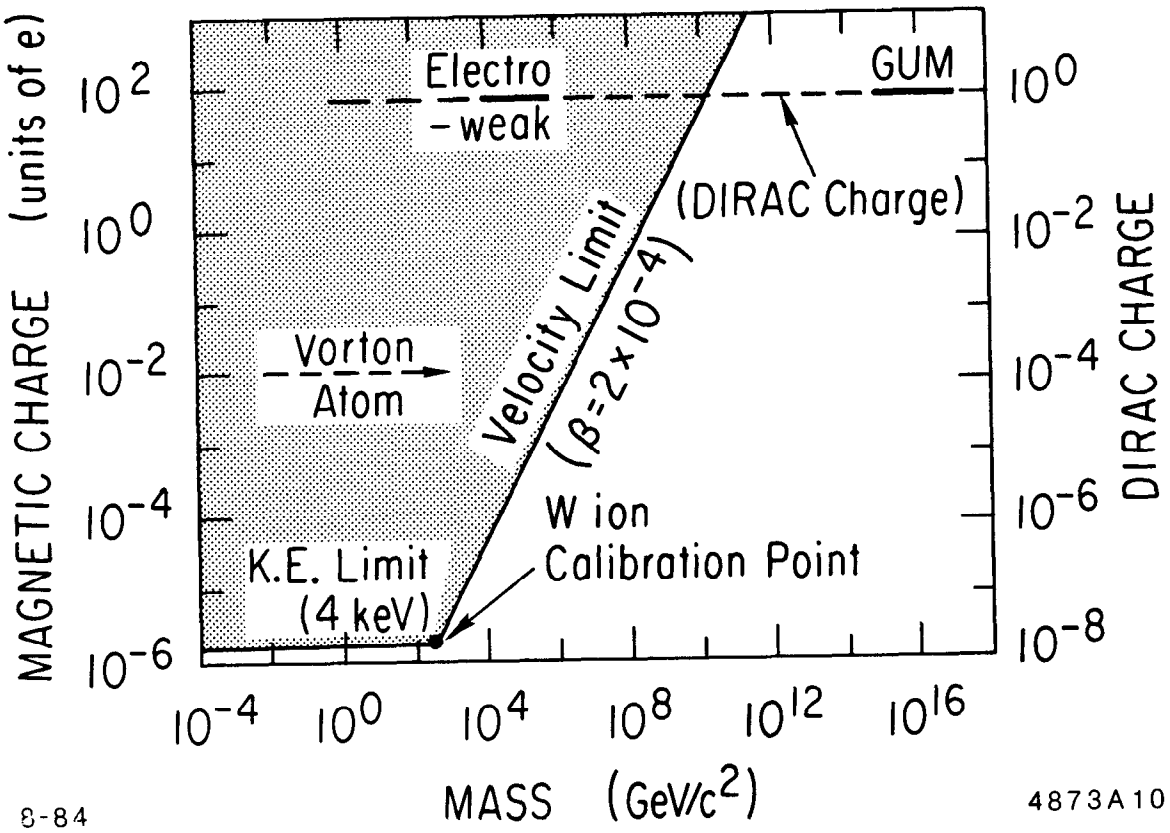
MAGNETIC CHARGE (units of e)
10^2
10^0
10^{-2}
10^{-4}
10^{-6}
Electro
-weak
GUM
(DIRAC Charge)
Vorton
Atom
Velocity Limit
(β=2x10^{-4})
W ion
Calibration Point
K.E. Limit
(4 keV)
10^{-4}
10^0
10^4
10^8
10^{12}
10^{16}
MASS (GeV/c^2)
10^0
10^{-2}
10^{-4}
10^{-6}
10^{-8}
DIRAC CHARGE
8-84
4873A10

Fig. 12